Switchless Tunable Bandstop-to-All-Pass Reconfigurable Filter

Eric J. Naglich, *Student Member, IEEE*, Juseop Lee, *Member, IEEE*, Dimitrios Peroulis, *Member, IEEE*, and William J. Chappell, *Senior Member, IEEE*

Abstract—The theory of a new type of bandstop-to-all-pass reconfigurable filter is developed in this work. A bandstop filter structure with both source-to-load and inter-resonator coupling is implemented. The synthesis equations are manipulated such that the signals in the filter's resonators and source-to-load transmission line can be made to constructively or destructively interfere at the output port through tuning of the resonant frequency of the filter's resonators. The relationship between resonator quality factor, filter bandwidth, and the all-pass response state is shown for the first time. The theory is proven through fabrication of a bandstop-to-all-pass filter with resonator unloaded quality factors greater than 500. Measured results show that the filter can continuously tune from insertion loss of 2.1 dB in the all-pass state to insertion loss of 69 dB in the bandstop state at the center frequency of the filter. Analog tuning of the attenuation level is also shown. The capability to switch from an all-pass to a variable-attenuation bandstop response enables a spectrally aware system to operate over wide bandwidths when interference levels are low and to dynamically add bandstop responses when interference affects its performance or signal equalization is required.

Index Terms—Filters, microwave filters, passive filters, tunable filters, tunable resonators.

I. INTRODUCTION

MOST past and current microwave front ends are primarily designed with bandpass filters for protection from generating or receiving unwanted interference [1]. One reason for the ubiquity of bandpass filters is that most microwave systems are unaware of the spectrum in which they are operating. This creates a need for a fear-based front-end architecture that attenuates all frequencies except the band of interest. However, a front-end architecture based on bandpass

filters can result in significant insertion loss in the frequency band of interest, limiting system performance. For a given resonator quality factor (Q), there is a tradeoff between bandpass filter bandwidth, order, and passband insertion loss [2]. Therefore, the greater the protection from generating or receiving interference in adjacent frequency bands, the higher the insertion loss in the band of interest.

A microwave system that is cognizant of the spectrum in which it is operating [3] would not need to operate in the fear-based mode of operation described above. In fact, it could use no filtering if there was not strong interference present. This would have the benefits of lower insertion loss than bandpass-centric front ends and much greater operating frequency flexibility. For example, a bandpass-centric system would need to switch between static filters in a bank [4], [5] or employ a tunable filter [6]–[9] to change operating frequencies. These methods involve a further increase in insertion loss due to the switch or a time delay due to filter tuning and shape adjustment, respectively. A front end without filtering has neither of these issues. In the event that interference became a concern, the spectrally aware system would know its frequency and could place a tunable bandstop filter [10]–[13] in its front-end frequency response to attenuate it. Employing tunable bandstop filters in spectrally aware systems minimizes insertion loss in the band of interest and maximizes the frequency range in which the system can instantaneously operate. Wideband systems [14] and systems with highly linear low-noise amplifiers (LNAs) [15] could benefit most from such an interference mitigation strategy. Allowing a receiver to take advantage of the benefits of a bandstop filter-centric front end while dynamically allowing for a mode of operation which allows signals at all frequencies to be received in low-power environments is the motivation of this work.

One way to have an open front-end frequency response in which bandstop filters can be added to on demand is to use bandstop filters that have a mode of operation that allows all frequencies to pass. This concept is shown in Fig. 1. Bandstop filters with this capability were shown in [16], [17], and [18]. However, the work in [16] uses superconducting structures and switches, which are not practical in some situations due to large volume and power requirements. The work in [17] also used switches in order to selectively add a parallel bandpass filter to the circuit which had a passband over the same frequency range as the stopband of the bandstop filter. The work in [18] achieves the desired effect without using switches for single-bandstop resonators which are twice-coupled to a through transmission line. Multipole filters are demonstrated in [18] by cascading the single-resonator structures. While the method in [18] achieves superior all-pass state insertion loss, it requires the use of long

Fig. 1. Concept and benefits of a bandstop-to-all-pass filter.

Fig. 2. Coupling routing diagram. $\mathrm{S} = \mathrm{source}, \mathrm{L} = \mathrm{load}, 1 = \mathrm{resonator}\,1, 2 = \mathrm{resonator}\,2$.

transmission lines and two tuning elements with each resonator. This paper presents the theory and measurement of switchless second-order bandstop filters that use series-coupled resonators to achieve bandstop-to-all-pass operation and attenuation level tuning, as well as the effect of finite resonator Q values on the all-pass response. In contrast to [18], the filter theory presented in this paper does not require coupling over large phase lengths of distributed resonators and can achieve a bandstop-to-all-pass response using a single tuning element per resonator. However, as noted above, the method in [18] produces less all-pass state insertion loss. This tradeoff between tuning complexity and all-pass state insertion loss makes both methods valuable. The measured filter was implemented with tunable highly loaded coaxial cavity resonators. These resonators have been used extensively by the authors and others to implement bandpass [19]–[21] and bandstop [22], [23] filters. However, it is important to note that the filter theory presented in this paper is applicable to filters using any type of tunable bandstop resonator.

II. BANDSTOP-TO-ALL-PASS FILTER THEORY

A. Bandstop and All-Pass State Responses

For the filters described in this paper, both external coupling values will be equal to each other, the resonator self-coupling values will have the same magnitude but opposite sign, and symmetries such as the source-to-load coupling being the same as the load-to-source coupling can be taken advantage of to simplify the generalized second-order filter $(N + 2) \times (N + 2)$ coupling matrix $\mathbf{M}$ to

$$\mathbf{M} = \begin{bmatrix} 0 & M_{01} & 0 & M_{03} \\ M_{01} & M_{11} & M_{12} & 0 \\ 0 & M_{12} & -M_{11} & M_{01} \\ M_{03} & 0 & M_{01} & 0 \end{bmatrix} \quad (1)$$

where the subscripts 0 and 3 correspond to the source and load, respectively, and the subscripts 1 and 2 correspond to the first and second resonator, respectively. Equation (1) corresponds to the coupling routing diagram shown in Fig. 2.
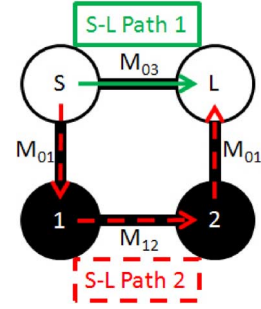
In [24], it was shown that a Butterworth bandstop filter response can be obtained from a structure with the coupling relationships in Fig. 2 if the correct relationship between M_{11} and M_{12} is maintained and M_{12} and M_{03} have the same sign. After substituting a value of positive one for M_{03} to represent coupling through a source-to-load inverter, the coupling relationships in (1) produce the transmission response

$$|S_{21}| = \left| \frac{s^2 + M_{11}^2 + M_{12}^2 - M_{01}^2 M_{12}}{s^2 + M_{01}^2 s + \frac{1}{2} M_{01}^4 + M_{11}^2 + M_{12}^2 - M_{01}^2 M_{12}} \right| \quad (2)$$

where s is the normalized frequency variable and is equal to $j\omega$, where j is the square root of -1 and ω is radian frequency. In [24], the transmission response in (2) was set equal to zero at a normalized frequency of zero to solve for the required relationship between M_{11} and M_{12} to produce a Butterworth bandstop response. If (2) is set equal to one, a solution exists not only at a normalized frequency of zero, but also at all frequencies if the resonators are synchronously tuned. In (1), synchronously tuned resonators are represented by an M_{11} value of zero. One set of solutions that results from setting (2) equal to one at all frequencies is

$$\begin{aligned} M_{01} &= \text{Arbitrary} \\ M_{12} &= \frac{M_{01}^2}{2} \\ M_{11} &= 0. \end{aligned} \quad (3)$$

With the relationship between M_{01} and M_{12} in (3) in place, the transmission response in (2) becomes

$$|S_{21}| = \left| \frac{s^2 + M_{11}^2 - \frac{M_{01}^4}{4}}{s^2 + M_{01}^2 s + M_{11}^2 + \frac{M_{01}^4}{4}} \right| \quad (4)$$

which has a magnitude of one for all values of $s = j\omega$ if M_{11} is zero. In other words, the magnitude of the numerator in (4) equals the magnitude of the denominator in (4) for all frequencies if the resonators are synchronously tuned. This is the all-pass state of the bandstop-to-all-pass filter.

However, the magnitude of (4) is not equal to one at all frequencies if M_{11} is set to a value other than zero. In addition, if (4) is set equal to zero at a normalized frequency of zero, there is a solution for M_{11}. The solution is

$$M_{11} = \frac{M_{01}^2}{2} \quad (5)$$

which yields the bandstop state of the bandstop-to-all-pass filter. In order for the bandstop state of the bandstop-to-all-pass filter to have the correct bandwidth in the normalized frequency domain, M_{01} should be set to a specific value for the desired filter shape. Any desired filter shape can be implemented since M_{01} can be arbitrary in the all-pass state of the filter according to (3). Therefore, setting M_{01} to correctly implement the bandstop filter state has no effect on the all-pass filter state.

In summary, if the relationship between M_{01} and M_{12} is designed correctly in a tunable second-order bandstop filter, the filter response can be switched between bandstop and all-pass states by merely tuning the resonant frequencies of the resonators so that M_{11} varies between zero and the value in (5). Frequency-scaled versions of the ideal synthesized bandstop and all-pass state responses according to the theory above can be seen in Fig. 1, where a second-order Butterworth response shape was chosen for the bandstop state of the filter. A second-order Butterworth bandstop filter requires an M_{01} of 1.189 [25].

B. Variable Attenuation and Bandwidth

If M_{11} is set to a value other than zero or the value in (5), other states of the filter are possible. If M_{11} is varied between zero and the value in (5), a bandstop filter response with variable bandwidth and attenuation results. This response could be useful in applications that require signal equalization. Additionally, if several filters of this type with different frequency tuning ranges were cascaded, the cascade could be dynamically reconfigured to provide frequency equalization, selective attenuation, or an all-pass response over very wide frequency ranges. If M_{11} is increased beyond the value in (5), a variable attenuation and bandwidth equi-ripple shape is achieved. The equiripple shape offers a wider bandwidth for a given level of attenuation than the Butterworth response, and the response can be tuned between these two states dynamically if tunable resonators are used. This greatly increases the flexibility of the filter. Example synthesized transmission responses and the associated M_{11} values can be seen in Fig. 3. The inset shows that the 10-dB bandwidth of the transmission response varies almost linearly with the scaling factor of M_{11} relative to the value in (5) over the range shown.

III. EFFECT OF FILTER BANDWIDTH AND FINITE UNLOADED QUALITY FACTOR ON ALL-PASS STATE RESPONSE

The bandstop-to-all-pass capability described in the previous section results from changing the value of the self-coupling M_{11} in the coupling matrix. Physically, this adjusts the phase response of the resonators by tuning along the reactance slope of their resonances. These changes in phase tune the interference between the filter's two source-to-load signals paths between constructive and destructive interference at the output port. The two signal paths can be seen in Fig. 2. In the ideal synthesis described in Section II, there was no loss in either of the source-to-load signal paths. Therefore, both perfect constructive and destructive interference were achieved in the synthesis equations. However, loss will exist in both signal paths in a fabricated filter, and the loss of each of the signal paths will not be equal in most real implementations. Different losses in the
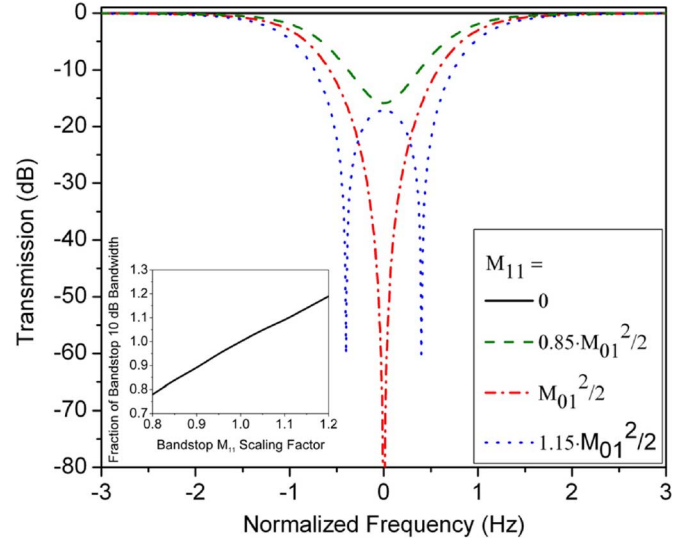

Fig. 3. Synthesized bandstop state response shapes as M_{11} is varied from the value in (5) by a scaling factor. Inset shows fraction of 10-dB bandwidth relative to the ideal Butterworth case (when M_{11} equals the value in (5)) versus M_{11} scaling factor relative to the M_{11} value in (5).

two source-to-load signal paths will have two main effects on a bandstop-to-all-pass filter's response. First, in the bandstop state, the filter will not produce infinite attenuation. This is the case for any real bandstop filter. Second, in the all-pass state, the signals from the two source-to-load paths will not perfectly reproduce the input signal at the output port. This lack of perfect signal reconstruction results in an unwanted all-pass state difference in passband insertion loss at the resonant frequency of the filter relative to non-resonant frequencies that is proportional to the difference in losses between the two source-to-load signal paths. The effect of imperfect signal reconstruction at the output port can be analyzed using a modification to (1). If the coupling mechanism that implements M_{03} in Fig. 2 is assumed to be lossless, a difference in loss between the two source-to-load signal paths can be completely modeled by assigning a finite resonator unloaded Q. A finite resonator unloaded Q can be added to (1) as

$$\mathbf{M} = \begin{bmatrix} 0 & M_{01} & 0 & M_{03} \\ M_{01} & -\frac{j}{Q_u \Delta} & M_{12} & 0 \\ 0 & M_{12} & -\frac{j}{Q_u \Delta} & M_{01} \\ M_{03} & 0 & M_{01} & 0 \end{bmatrix} \tag{6}$$

where Q_u is resonator-unloaded Q and Δ is the 3-dB fractional bandwidth. The larger Q_u and Δ are, the closer the response of (6) will become to the ideal response of (1). Although this analysis uses a lossless coupling mechanism for M_{03}, it approximates reality well because M_{03} is frequently implemented with a low-loss transmission line in bandstop filters.

While (6) shows that Δ and/or Q_u can be increased in order to improve the all-pass state response of a bandstop-to-all-pass filter, Δ is usually set by specific application requirements. Similarly, specific application requirements will require a maximum all-pass state insertion loss, which dictates the Q_u needed. The second-order Butterworth filter equation of the required Q_u for
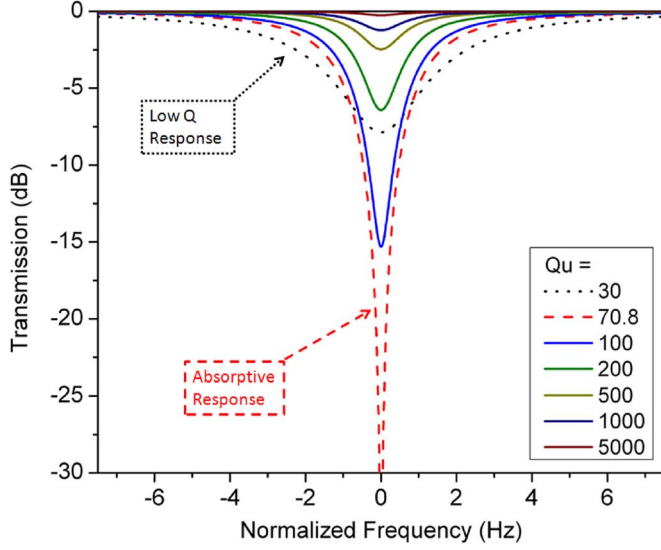
Fig. 4. Synthesized all-pass state responses for a 2% fractional bandwidth bandstop filter for various unloaded Q values. In all responses, the return loss is 0 ($-\infty$ dB).

Fig. 5. Simulation model of the fabricated bandstop-to-all-pass filter.

a specified Δ and a desired level of all-pass state insertion loss can be derived from (6), and it is

$$Q_u = \frac{1}{1.414\Delta \left(\frac{1}{|S_{21(0)}|+1} - \frac{1}{2} \right)} \qquad (7)$$

where $S_{21(0)}$ is the insertion loss at $s = 0$ in linear scale. For example, if Δ is required to be 2%, (6) produces the normalized frequency-domain all-pass state transmission responses in Fig. 4 as Q_u is varied. Note that all of the responses in Fig. 4 have a theoretically perfect impedance match to the ports of the system. Fig. 4 shows that, with very high Q_u values, the response approaches the ideal lossless case described in Section II. As Q_u is lowered, the all-pass state has more and more insertion loss until a special case is reached. This special case is an absorptive bandstop filter [26]–[28], which has theoretically infinite attenuation in its stopband and is perfectly impedance matched at all frequencies. The high Q_u examples are shown with solid traces in Fig. 4, while the absorptive case is designated by a dashed trace. The dotted trace in Fig. 4 shows an example of the wide, shallow response that occurs when Q_u is below the value that produces the absorptive response. The responses in Fig. 4 demonstrate that in order to implement a bandstop-to-all-pass filter with the best all-pass state for a given Δ, high-Q tunable resonators are required. Finally, while this paper presents theory for a two-pole bandstop filter, the analysis for higher-order filters is similar. It is important to note that the all-pass state insertion loss due to finite-Q_u resonators described above accumulates for higher order filters.

IV. FILTER DESIGN AND FABRICATION

Evanescent-mode cavity resonators have been shown to have wide tuning ranges while retaining high Q values [19], [20], [29]. These traits make them very well suited for use in realizations of bandstop-to-all-pass filters. In order to verify the
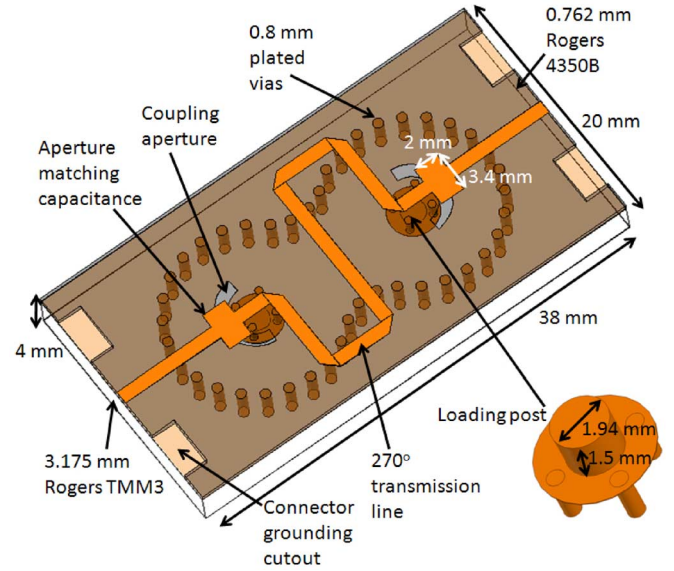
theory in Sections II and III, an evanescent-mode cavity based, second-order filter was designed and fabricated. A model of the filter with dimensional annotations can be seen in Fig. 5. The filter includes three copper layers and two dielectric layers.

The top copper layer in Fig. 5 is the source-to-load transmission line. In this implementation, a 270° transmission line at 3 GHz was chosen in order to match the sign of its coupling to the sign of the inter-resonator coupling as required by (1). The inter-resonator coupling and its sign will be explained further below. The source-to-load transmission line also employs capacitive patches to improve impedance matching in the filter's upper passband as described in [23]. The top dielectric layer of the filter structure is a 0.762-mm-thick sheet of Rogers 4350B material ($\epsilon_r = 3.66$, $\tan(\delta) = 0.0037$ @ 10 GHz) that has rectangles cut out of it to facilitate grounding of the input and output connectors.

The second copper layer of the structure is the ground plane for the source-to-load transmission line. This copper layer also contains coupling apertures that couple the mode of the source-to-load transmission line to the mode of the cavity resonators. These coupling apertures were sized and optimized in simulation to produce the correct amount of coupling for a 2.5% fractional bandwidth Butterworth response [30]. The second dielectric layer of the structure is a 3.175-mm-thick sheet of Rogers TMM3 material ($\epsilon_r = 3.27$, $\tan(\delta) = 0.002$ @ 10 GHz) that contains the evanescent-mode cavity resonators. The two dielectric layers of the structure were bonded together using DuPont Pyralux LFO100 adhesive. The cavity walls are formed by 0.8-mm-diameter copper-plated vias, and the cavity diameter is 13.6 mm from the center of one via to the center of the opposite via. The cavities have copper-plated loading posts that are 1.94 mm in diameter and 1.5 mm tall. These loading posts are supported on a copper platform that is connected to the top of the cavity in Fig. 5 by four plated vias. The inset in Fig. 5 shows the geometry of the loading posts inverted with respect to their orientation in the full structure shown in Fig. 5 for clarity.
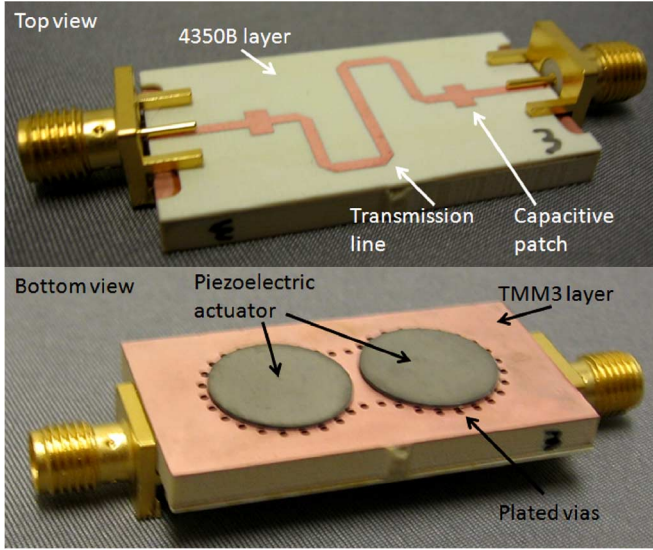
Fig. 6.   Top and bottom views of the fabricated bandstop-to-all-pass filter.

Fig. 7.   Measured bandstop and all-pass states of the fabricated bandstop-to-all-pass filter.

Inter-resonator coupling is implemented through an iris between the two cavities. The iris was designed in simulation to produce the correct M_{12} value according to (5) [31]. Iris coupling, which is predominantly magnetic field coupling, was chosen because of the field distribution in evanescent-mode cavities. Since most of the electric field in the cavity is concentrated in the gap above the loading post, the magnetic field is much more accessible. The inter-resonator coupling can be modeled as an inductive T network that has an insertion phase that approaches 90°. This requires a 270° electrical length source-to-load transmission line in order to properly implement (1) and have the same sign coupling for both M_{03} and M_{12}. However, evanescent-mode cavity compatible inter-resonator coupling structures that provide the opposite sign coupling compared with the iris implemented in this work exist [32]. The third copper layer of the structure is a thin copper membrane that is laminated to the TMM3 layer everywhere except within the boundaries of the cavity walls. This allows the thin copper membrane to flex above the loading posts. Attached to the side of the flexible copper membranes external to the cavity using silver epoxy are 0.38-mm-thick, 1/2-in-diameter piezoelectric actuators from Piezo Systems, Inc. The piezoelectric actuators allow electronic control of the gaps between the loading posts in the resonators and the flexible copper membrane, which changes the resonant frequency of each resonator. Images of the fabricated filter can be seen in Fig. 6. Fig. 6 clearly shows the positioning of the piezoelectric actuators.

V. MEASURED RESULTS

The response of the fabricated bandstop-to-all-pass filter was measured using an Agilent Technologies N5230C PNA. Bias voltages were applied to the piezoelectric actuators using Keithley 2400 Sourcemeters. The final structure was simulated using Ansoft HFSS. Measured results of the bandstop and all-pass states of the fabricated filter can be seen in Fig. 7. Fig. 7 shows a 2.1-dB insertion loss in the all-pass state at
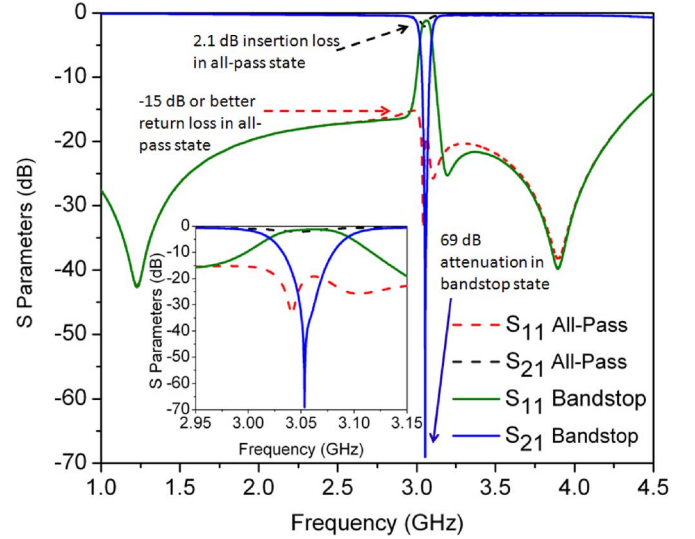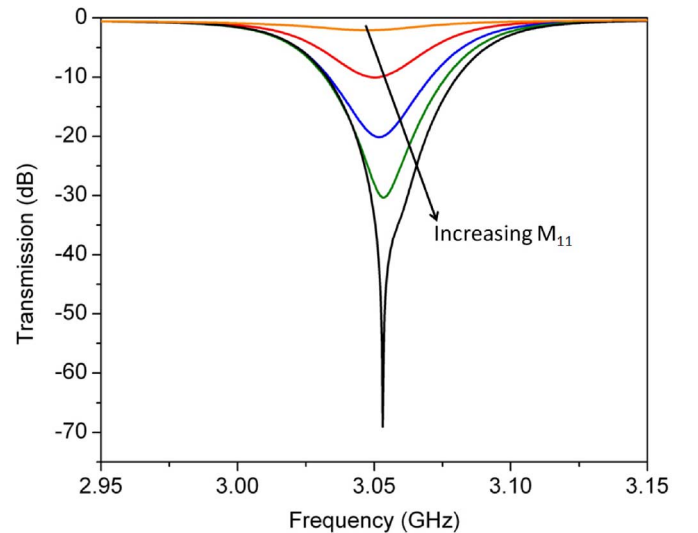

Fig. 8.   Measured 2.1-, 10-, 20-, 30-, and 70-dB attenuation states of the fabricated bandstop-to-all-pass filter.

3.05 GHz. When the resonators are tuned away from 3.05 GHz, the response has insertion loss of 0.4 dB. Therefore, the all-pass state resonances provide an additional insertion loss of 1.7 dB at 3.05 GHz in the all-pass state. A 15-dB or greater return loss is maintained from 1 to 4.25 GHz, and the response approximates a through transmission line. In the bandstop state, attenuation of 69 dB is shown, and the 3-dB fractional bandwidth is 2.7%. According to the theory in Section III, this fractional bandwidth and all-pass level of attenuation corresponds to a resonator Q of 540, which is in line with Q's of previously reported, similarly sized evanescent-mode cavity resonators [29]. The response is also able to be tuned to any attenuation level between 2.1 and 69 dB shown in Fig. 7 by tuning the resonant frequencies of the resonators. For example, tuning M_{11} to the value in (5) results in the 69-dB attenuation response. Fig. 8 shows the 2.1-, 10-, 20-, 30-, and 70-dB attenuation responses of the fabricated
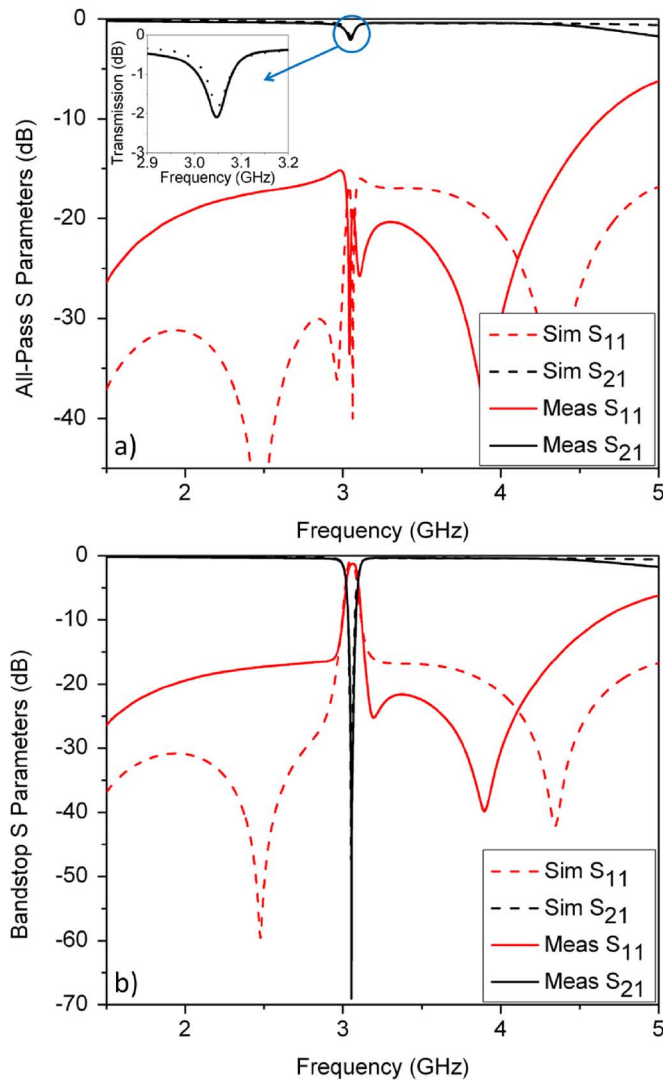
Fig. 9. Measured versus simulated S-parameters for the bandstop-to-all-pass filter. (a) All-pass state. (b) Bandstop state.
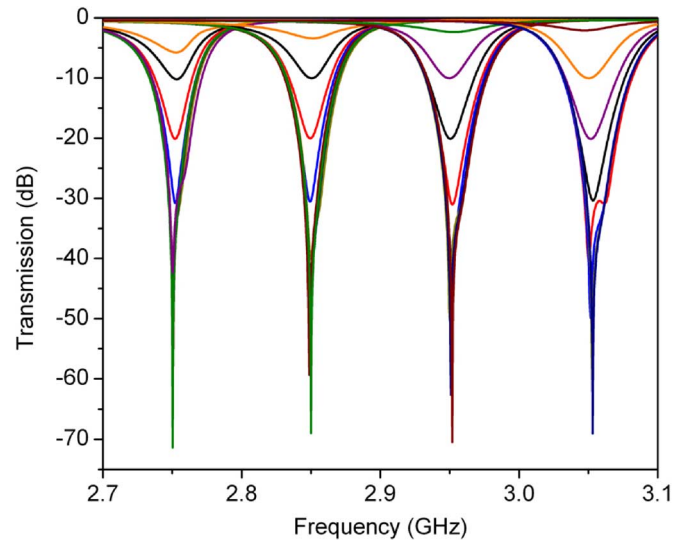

Fig. 10. Several measured response states of a single filter tuning from 2.75 to 3.1 GHz. Less than 4-, 10-, 20-, 30-, 40-, 50-, 60-, and 70-dB attenuation states are shown. Note that the center frequency of the filter is continuously tunable over the entire range.

filter. This functionality would be useful in applications that require signal equalization.

Measured versus simulated S_{11} and S_{21} responses can be seen in Fig. 9. In the all-pass state, the measured insertion loss at the resonant frequency of the resonators is 2.1 dB versus a simulated value of 1.8 dB. This difference is due to the lower quality factor of the fabricated resonators compared to the simulated resonators which can result from copper surface roughness and oxidation. Connector losses also contribute to the difference in insertion losses. The measured filter's upper passband starts to degrade at lower frequencies compared with the simulated filter. The degradation is the result of an impedance mismatch caused by the coupling apertures in the ground plane of the source-to-load transmission line. Imperfections in the size of the coupling apertures or the capacitive matching patches in the feeding microstrip transmission line relative to the simulated geometry produce lower frequency passband degradation like what is shown in Fig. 9(a). However, the measured performance matches the simulated performance well in the band of interest. In the bandstop filter state shown in Fig. 9(b), the measured 3-dB

fractional bandwidth is 2.7% versus a simulated value of 2.5%. This difference supports the theory above that the coupling apertures may have been fabricated to be a slightly incorrect size. In addition, the measured reflection zeros are not at the same frequencies at which they appear in the simulated response, further supporting an unmodeled impedance mismatch at either the coupling slots or the connector-to-microstrip transition. While fabrication process limitations resulted in 50 to 200 μm of inaccuracy, the shape and attenuation levels of the measured bandstop response still match simulated results well and prove the bandstop-to-all-pass concept. Standard professional fabrication facilities would be able to reduce these inaccuracies greatly.

The lowest measured all-pass state insertion loss, 2.1 dB, was achieved at 3.05 GHz. However, the all-pass response, as well as the variable attenuation capability shown in Fig. 8, can be continuously tuned over the range of 2.75 to 3.1 GHz with insertion loss less than 4 dB in the all-pass state. Fig. 10 shows measurements of many of the possible response shapes in this band. The filter is continuously tunable in both frequency and attenuation from 2.75 to 3.1 GHz and from 2.1 to 70 dB, respectively. In addition to the many shapes shown in Fig. 10, equiripple responses were also measured. In Fig. 11, 10- and 20-dB equiripple responses can be seen. These responses were obtained through tuning M_{11} beyond the value in (5), and a larger M_{11} resulted in a wider bandwidth response. Such equiripple responses can be achieved by many tunable bandstop filters when the resonances are slightly offset from each other in frequency, and they are not a unique aspect of the bandstop-to-all-pass filter. The equiripple responses result from interaction of the edges of the stopbands of the resonances. The 3-dB fractional bandwidth of the 3.05-GHz 10-dB equiripple response is 3.8%, and that of the 3.05-GHz 20-dB equiripple response is 3.1%. Since these responses are wider than the responses shown above, this capability allows a dynamic tradeoff between filter bandwidth and level of attenuation. The measured responses in Figs. 7–11 are comparable to the theoretical responses in Figs. 3
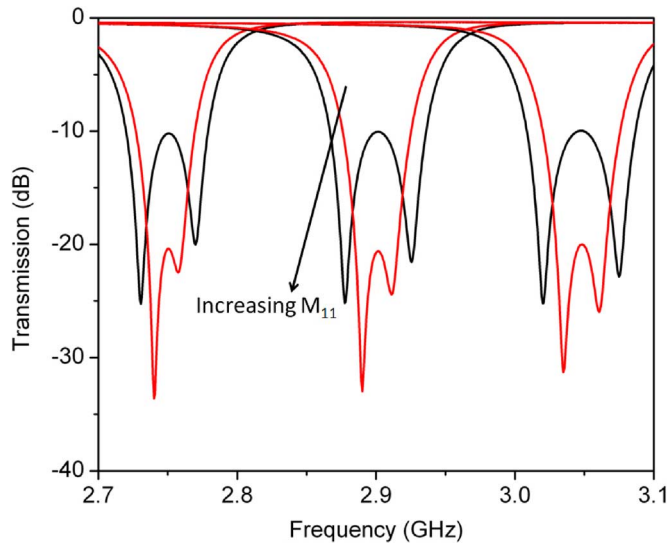
Fig. 11. Measured 10- and 20-dB equiripple responses. The capability to provide this response shape allows a tradeoff between attenuation level and bandwidth.

and 4, proving the effect of finite resonator Q and tuning of M_{11} for the bandstop-to-all-pass filter theory presented in this work. It is important to note that changing between all-pass, Butterworth bandstop, and equiripple bandstop filter shapes requires only very slight frequency tuning of the resonators. Subject to the tuning speed of the resonators used in a particular implementation of a bandstop-to-all-pass filter, the filter shape could be reoptimized very quickly should the spectrum or signals of interest change.

VI. CONCLUSION

An electronically reconfigurable bandstop-to-all-pass filter was shown that can provide numerous response shapes for spectrally aware systems. The theory of such a filter was developed through the use of coupling matrices such that only the resonator center frequencies need to be tuned in order to achieve bandstop-to-all-pass reconfiguration. In the filter's bandstop state, 70 dB of attenuation was measured with a 3-dB bandwidth of 2.7%. The attenuation level was able to be continuously varied over a very wide range, and equi-ripple responses were also demonstrated. In the filter's all-pass state, the filter had 0.14-0.74 dB of passband insertion loss from 1 to 4.25 GHz and an insertion loss of 2.1 dB at the filter's center frequency.

Applications of a bandstop-to-all-pass reconfigurable filter are envisioned to include wide operating bandwidth, cognitive systems. With bandstop-to-all-pass filters, a system could configure its front end response to the all-pass state when interference was limited, reducing insertion loss compared to bandpass filter front end designs. When interference started to affect performance, the system could place bandstop responses in its front end response at the frequencies of the interference. In addition, a cascade of bandstop-to-all-pass filters could provide the functionality described in this paper over multi-octave frequency ranges. The filtering capability and flexibility provided by bandstop-to-all-pass filters enables new high-frequency front end strategies featuring very low passband insertion loss.

REFERENCES

[1] I. Hunter, R. Ranson, A. Guyette, and A. Abunjaileh, "Microwave filter design from a systems perspective," *IEEE Microw. Mag.*, vol. 8, no. 5, pp. 71–77, Oct. 2007.

[2] I. Hunter, *Theory and Design of Microwave Filters*. London, U.K.: Inst. Electr. Eng., 2001, ch. 4, pp. 125–131.

[3] B. Perlman, J. Laskar, and K. Lim, "Fine-tuning commercial and military radio design," *IEEE Microw. Mag.*, vol. 9, no. 4, pp. 95–106, Aug. 2008.

[4] J. Slobodnik, A. J. , G. Roberts, J. Silva, W. Kearns, J. Sethares, and T. Szabo, "Switchable SAW filter banks at UHF," *IEEE Trans. Sonics Ultrason.*, vol. SU-26, no. 2, pp. 120–126, Mar. 1979.

[5] J. Liu, S. He, S. Li, J. Liu, and Y. Liang, "P6G-3 switchable SAW filter bank with both narrow & wide channel bandwidth and 10 channels SAW filter bank," in *Proc. IEEE Ultrason. Symp.*, Oct. 2007, pp. 2578–2581.

[6] X. Y. Zhang and Q. Xue, "High-selectivity tunable bandpass filters with harmonic suppression," *IEEE Trans. Microw. Theory Tech.*, vol. 58, no. 4, pp. 964–969, Apr. 2010.

[7] L.-H. Hsieh and K. Chang, "Tunable microstrip bandpass filters with two transmission zeros," *IEEE Trans. Microw. Theory Tech.*, vol. 51, no. 2, pp. 520–525, Feb. 2003.

[8] J. Nath, D. Ghosh, J.-P. Maria, A. Kingon, W. Fathelbab, P. Franzon, and M. Steer, "An electronically tunable microstrip bandpass filter using thin-film barium-strontium-titanate (BST) varactors," *IEEE Trans. Microw. Theory Tech.*, vol. 53, no. 9, pp. 2707–2712, Sep. 2005.

[9] K. Entesari and G. Rebeiz, "A differential 4-bit 6.5–10-GHz RF MEMS tunable filter," *IEEE Trans. Microw. Theory Tech.*, vol. 53, no. 3, pp. 1103–1110, Mar. 2005.

[10] I. Reines, S.-J. Park, and G. Rebeiz, "Compact low-loss tunable X-band bandstop filter with miniature RF-MEMS switches," *IEEE Trans. Microw. Theory Tech.*, vol. 58, no. 7, pp. 1887–1895, Jul. 2010.

[11] W. Yan and R. Mansour, "Compact tunable bandstop filter integrated with large deflected actuators," in *IEEE MTT-S Int. Microw. Symp. Dig.*, Jun. 2007, pp. 1611–1614.

[12] C. Tsai, G. Qiu, H. Gao, L. Yang, G. Li, S. Nikitov, and Y. Gulyaev, "Tunable wideband microwave band-stop and bandpass filters using YIG/GGG-GaAs layer structures," *IEEE Trans. Magn.*, vol. 41, no. 10, pp. 3568–3570, Oct. 2005.

[13] C. Rauscher, "Varactor-tuned active notch filter with low passband noise and signal distortion," *IEEE Trans. Microw. Theory Tech.*, vol. 49, no. 8, pp. 1431–1437, Aug. 2001.

[14] C. Rodenbeck, S.-G. Kim, W.-H. Tu, M. Coutant, S. Hong, M. Li, and K. Chang, "Ultra-wideband low-cost phased-array radars," *IEEE Trans. Microw. Theory Tech.*, vol. 53, no. 12, pp. 3697–3703, Dec. 2005.

[15] K. Kobayashi, Y. C. Chen, I. Smorchkova, R. Tsai, M. Wojtowicz, and A. Oki, "A 2 watt, sub-dB noise figure GaN MMIC LNA-PA amplifier with multi-octave bandwidth from 0.2–8 GHz," in *IEEE MTT-S Int. Microw. Symp. Dig.*, Jun. 2007, pp. 619–622.

[16] K. Raihn, N. Fenzi, G. Hey-Shipton, E. Saito, V. Loung, and D. Aidnik, "Adaptive high temperature superconducting filters for interference rejection," *IEEE Trans. Microw. Theory Tech.*, vol. 44, no. 7, pp. 1374–1381, Jul. 1996.

[17] J. Rhodes, "Switched bandstop filters," *Int. J. Circuit Theory Applic.*, vol. 22, pp. 107–120, 1994.

[18] A. Guyette, "Varactor-tuned bandstop filters with tunable center frequency and bandwidth," in *Proc. IEEE Int. Conf. Wireless Inf. Technol. Syst.*, Sep. 3, 2010, pp. 1–4, 28 2010–.

[19] X. Liu, L. Katehi, W. Chappell, and D. Peroulis, "High- tunable microwave cavity resonators and filters using soi-based rf mems tuners," *J. Microelectromech. Syst.*, vol. 19, no. 4, pp. 774–784, Aug. 2010.

[20] H. Joshi, H. Sigmarsson, S. Moon, D. Peroulis, and W. Chappell, "High- Q fully reconfigurable tunable bandpass filters," *IEEE Trans. Microw. Theory Tech.*, vol. 57, no. 12, pp. 3525–3533, Dec. 2009.

[21] Z.-C. Hao, W. Hong, J.-X. Chen, X.-P. Chen, and K. Wu, "Compact super-wide bandpass substrate integrated waveguide (SIW) filters," *IEEE Trans. Microw. Theory Tech.*, vol. 53, no. 9, pp. 2968–2977, Sep. 2005.

[22] E. Naglich, J. Lee, D. Peroulis, and W. Chappell, "High-Q tunable bandstop filters with adaptable bandwidth and pole allocation," in *IEEE MTT-S Int. Microw. Symp. Dig.*, Jun. 2011, pp. 1–4.

[23] E. Naglich, J. Lee, D. Peroulis, and W. Chappell, "Extended passband bandstop filter cascade with continuous 0.85–6.6-GHz coverage," *IEEE Trans. Microw. Theory Tech.*, vol. 60, no. 1, pp. 21–30, Jan. 2012.

[24] J. Lee, E. Naglich, and W. Chappell, "Frequency response control in frequency-tunable bandstop filters," *IEEE Microw. Wireless Compon. Lett.*, vol. 20, no. 12, pp. 669–671, Dec. 2010.

[25] E. Naglich, J. Lee, D. Peroulis, and W. Chappell, "A tunable bandpass-to-bandstop reconfigurable filter with independent bandwidths and tunable response shape," *IEEE Trans. Microw. Theory Tech.*, vol. 58, no. 12, pp. 3770–3779, Dec. 2010.

[26] D. Jachowski, "Compact, frequency-agile, absorptive bandstop filters," in *IEEE MTT-S Int. Microw. Symp. Dig.*, Jun. 2005, pp. 513–516.

[27] M. Morgan and T. Boyd, "Theoretical and experimental study of a new class of reflectionless filter," *IEEE Trans. Microw. Theory Tech.*, vol. 59, no. 5, pp. 1214–1221, May 2011.

[28] I. Hunter, A. Guyette, and R. Pollard, "Passive microwave receive filter networks using low-Q resonators," *IEEE Microw. MAg.*, vol. 6, no. 3, pp. 46–53, Sep. 2005.

[29] H. Joshi, H. Sigmarsson, D. Peroulis, and W. Chappell, "Highly loaded evanescent cavities for widely tunable high-Q filters," in *IEEE MTT-S Int. Microw. Symp. Dig.*, Jun. 2007, pp. 2133–2136.

[30] A. Khanna and Y. Garault, "Determination of loaded, unloaded, and external quality factors of a dielectric resonator coupled to a microstrip line," *IEEE Trans. Microw. Theory Tech.*, vol. MTT-31, no. 3, pp. 261–264, Mar. 1983.

[31] A. Atia and A. Williams, "Measurements of intercavity couplings (short papers)," *IEEE Trans. Microw. Theory Tech.*, vol. MTT-23, no. 6, pp. 519–522, Jun. 1975.

[32] J. Lee, E. Naglich, H. Sigmarsson, D. Peroulis, and W. Chappell, "Tunable inter-resonator coupling structure with positive and negative values and its application to the field-programmable filter array (FPFA)," *IEEE Trans. Microw. Theory Tech.*, vol. 59, no. 12, pp. 3389–3400, Dec. 2011.

RF and microwave components, satellite transponders, and electromagnetic theories.

Dr. Lee was a recipient of the Highest Honor Award presented by Korea University, the Undergraduate Fellowship presented by Korea University, the Graduate Fellowship presented by LG Information and Communications, and the Graduate Fellowship presented by Korea Science and Engineering Foundation. He was a recipient of the Rackham Predoctoral Fellowship presented by Rackham Graduate School, The University of Michigan. He was also the recipient of the IEEE Microwave Theory and Techniques Society (IEEE MTT-S) Graduate Fellowship. His coauthored paper received the second place award in the 2010 IEEE MTT-S International Microwave Symposium Student Paper Competition. He is listed in *Who's Who in America*.

Dimitrios Peroulis (S'99–M'04) received the Ph.D. degree in electrical engineering from The University of Michigan at Ann Arbor in 2003.

He has been with Purdue University, West Lafayette, IN, since August 2003, where he is currently leading a group of graduate students on a variety of research projects in the areas of RF MEMS, sensing and power-harvesting applications, as well as RFID sensors for the health monitoring of sensitive equipment. He has been a Principal Investigator (PI) or a co-PI in numerous projects funded by government agencies and industry in these areas. He is currently a key contributor in two Defense Advanced Research Projects Agency (DARPA) projects at Purdue focusing on very high-quality ($Q > 1\,000$) RF tunable filters in mobile form factors (DARPA Analog Spectral Processors Program, Phases I, II and III) and on developing comprehensive characterization methods and models for understanding the viscoelasticity/creep phenomena in high-power RF MEMS devices (DARPA M/NEMS S&T Fundamentals Program, Phases I and II). Furthermore, he is leading the experimental program on the Center for the Prediction of Reliability, Integrity and Survivability of Microsystems (PRISM) funded by the National Nuclear Security Administration. In addition, he is heading the development of the MEMS technology in a U.S. Navy project (Marines) funded under the Technology Insertion Program for Savings (TIPS) program focused on harsh-environment wireless micro-sensors for the health monitoring of aircraft engines. He has authored or coauthored over 110 refereed journal and conference publications in the areas of microwave integrated circuits and antennas.

Dr. Peroulis received the National Science Foundation CAREER award in 2008. His students have received numerous student paper awards and other student research-based scholarships. He has also received eight teaching awards including the 2010 HKN C. Holmes MacDonald Outstanding Teaching Award and the 2010 Charles B. Murphy award, which is Purdue University's highest undergraduate teaching honor.

Eric J. Naglich (S'09) received the B.S.E.C.E. degree from Purdue University, West Lafayette, IN, in 2007, where he is currently working toward the Ph.D. degree in electrical and computer engineering under the direction of Prof. W. J. Chappell and Prof. D. Peroulis.

He was with GE Healthcare from 2007 to 2009, where he was involved with electromagnetic subsystem design in medical imaging and surgical navigation machines during the Edison Engineering Development Program. His current research focuses on tunable filter synthesis and fabrication for widely tunable, adaptive RF front ends in cognitive radio and radar applications.

Mr. Naglich is a member of the IEEE Microwave Theory and Techniques Society (IEEE MTT-S), the president of the Purdue MTT-S student chapter, and a past officer of Purdue University's Beta chapter of Eta Kappa Nu. His paper received the second place award in the 2010 IEEE MTT-S International Microwave Symposium Student Paper Competition.

Juseop Lee (A'02–M'03) received the B.E. and M.E. degrees in radio science and engineering from Korea University, Seoul, Korea, in 1997 and 1999, respectively, and the Ph.D. degree in electrical engineering from The University of Michigan, Ann Arbor, in 2009.

In 1999, he joined LG Information and Communications (now LG Electronics), Korea, where his activities included design and reliability analysis of RF components for code-division multiple-access (CDMA) cellular systems. In 2001, he joined Electronics and Telecommunications Research Institute (ETRI), Korea, where he was involved in designing passive microwave equipment for Ku- and Ka-band communications satellites. In 2005, he joined The University of Michigan at Ann Arbor, where he was a Research Assistant and Graduate Student Instructor with the Radiation Laboratory, and his research activities focused on millimeter-wave radars and synthesis techniques for multiple-passband microwave filters. In 2009, he joined Purdue University, West Lafayette, IN, where he was a Post-Doctoral Research Associate, and his activities included the design of adaptable RF systems. In 2012, he joined the Department of Computer and Communications Engineering, Korea University, Korea, Seoul, where he is currently an Assistant Professor. His research interests include

William J. Chappell (S'98–M'02–SM'10) received the B.S.E.E., M.S.E.E., and Ph.D. degrees from The University of Michigan at Ann Arbor in 1998, 2000, and 2002, respectively.

He is currently an Associate Professor with the School of Electrical and Computer Engineering, Purdue University, West Lafayette, IN, where he is also a Member of the Birck Nanotechnology Center and the Center for Wireless Systems and Applications. His research focus is on advanced applications of RF and microwave components. He has been involved with numerous Defense Advanced Research Projects Agency (DARPA) projects involved in advanced packaging and material processing for microwave applications. His research sponsors include HSARPA, the Office of Naval Research, the National Science Foundation, the state of Indiana, CERDEC, and ARO, as well as industry sponsors. His research group uses electromagnetic analysis, unique processing of materials, and advanced design to create novel microwave components. His specific research interests are the application of very high-quality and tunable components utilizing multilayer packages. In addition, he is involved with high-power RF systems, packages, and applications.

Dr. Chappell was the IEEE Microwave Theory and Techniques Society (IEEE MTT-S) Administrative Committee (AdCom) secretary for 2009 and was elected to the IEEE MTT-S AdCom for 2010–2012.